Multidimensional ECC Behaviors of Air-Water Flow in a Downcomer Annulus with Direct Vessel Injection Mode during the LBLOCA Reflood Phase

Xin Ma [1,2], Wan Sun [* 1,2], Jie Wan [1,2], Yang Liu [1,2], Zhanghao Zhu [1,2], Huafa Chen [3],Luteng Zhang [1,2], Zaiyong Ma [1,2], Liangming Pan [1,2]

1. Key Laboratory of Low-Grade Energy Utilization Technologies and Systems, Ministry of Education, Chongqing University, Chongqing 400044, PR China
2. Department of Nuclear Engineering and Nuclear Technology, Chongqing University, Chongqing 400044, PR China
3. Nuclear Power Technology Research Institute Co.,Ltd, Shenzhen of Guangdong Prov. 518000, China

* Corresponding author: Email address: sunwan@cqu.edu.cn

Abstract： The direct vessel injection (DVI) technology has been increasingly adopted in new pressurized water reactors due to its advantages in simplifying the safety injection system design and enhancing economic benefits. This study focuses on the modified DVI safety injection system of the HPR1000. An improved linear scaling method was employed to model the prototype, and relevant experiments were conducted on a 1:8.5 scale visualization test section. During the refilling and reflooding stages of a large break loss - of - coolant accident (LBLOCA), phenomena such as counter current flow limitation (CCFL) and bypass flow near the break were observed within the annular cavity. The research investigated the impacts of various break locations and the presence or absence of guiding structures on the bypass effect in the DVI safety injection system. Additionally, comparisons were made between DVI safety injection and cold - leg injection. The findings reveal that direct bypass flow dominates the safety injection bypass during the refilling and reflooding stages of an LBLOCA. The closer the cold - leg break location is to the DVI nozzle, the more significant the increase in bypass flow at the break location. Different DVI injection heights affect the spread of the liquid film, thereby influencing the proportion of bypass flow. The installation of guiding devices can effectively reduce the proportion of safety injection bypass flow. The data results of this study provide crucial insights for the optimization and innovation of the modified safety injection system in HPR1000.

KEYWORDS

Direct vessel injection (DVI), Improved linear scaling, Counter-current flow limitation (CCFL), Large break loss-of-coolant accident (LBLOCA), Direct bypass flow

1.Introduction

Undoubtedly, with a growing world population, economic expansion and rising expectations of living standards, the demand for clean energy and a sustainable environment will continue to increase[1]. Nuclear energy as a clean and efficient renewable energy has been greatly developed, at the same time, nuclear safety issues are also concerned. Large break loss of coolant accident (LBLOCA) is a critical nuclear accident in pressurized water reactor (PWR) systems. Under certain conditions, the steam in the annular descent section of the pressure vessel can cause the safe injection liquid to either fail to flow down completely or bypass the annulus cavity to reach the rupture position of the cold pipe section, leading to the phenomenon of counter current flow limitation (CCFL) [2,3]. The two - phase countercurrent restriction determines the bypass flow rate of the emergency core coolant, which in turn determines the flow rate of the return coolant[4].

In recent years, numerous scholars have conducted extensive numerical simulation and experimental studies to develop and validate multidimensional safety analysis procedures, aiming to more realistically simulate the two - phase flow phenomenon in nuclear reactors during LBLOCA. For instance, Yun et al. [5] utilized air - water as the medium on a 1/7.5 UPTF test bench to study the multidimensional characteristics of two - phase flow in the descending section geometry. Dong Won LEE et al. [6] conducted water film spreading, purging, and direct ECC side - flow tests on a 1/7 APR1400 device, investigated the ECC water film behavior in the descending section, and verified the applicability of the improved linear proportional modeling method and the linear proportional modeling method. H.K. Cho et al. [7] carried out a series of experiments on the 1/7.3 - 1/4 ratio UPTF and 1/7 - 1/5 ratio APR 1400 declining sections, studied the impact of geometric structure on the side flow characteristics, and analyzed the results of each structure using the Wallis number as a dimensionless number. In addition, many scholars at home and abroad have also carried out relevant studies under different structural sizes[8-20]. Some scholars have also carried out a large number of studies using systematic procedures or numerical simulation methods. [21-23]

However, most existing studies are still centered around the bypass phenomenon in the safe injection mode of the cold pipe section. The improved safety injection system of the third - generation advanced nuclear reactor HPR1000, independently developed by China, intends to adopt the pressure vessel direct injection (DVI) method. This approach can simplify the safety injection system design and improve economic efficiency while ensuring safety. Third - generation pressurized water reactor nuclear power plants such as AP1000 [24,25] in the United States, APR1400 [26] in South Korea, and VVER1000 [27] in Russia, as well as a number of second -

generation improved pressurized water reactor nuclear power plants under construction in China, all employ this technology. Nevertheless, the use of DVI technology leads to a significant increase in the flow rate of safe water injection, and its entraining and direct ECC bypass behaviors differ from those of the traditional cold pipe section. Therefore, it is necessary to conduct multidimensional experimental research on the ECC behavior in the DVI mode decline section. Moreover, due to the differences in the geometry of the UPTF and APR1400 compared to that of the HPR1000 improved safety injection system, the relevant data cannot be directly applied to the safety assessment of the HPR1000 system. Liang Xiao [28]and Xiao Weiming et al. [29] have studied the original HPR1000 safety injection system, but the results can not be directly used in the improved safety injection system.

To address this issue, this paper introduces the hydraulic characteristics of ECC and the action mechanism of ECC bypass in the DVI system downcomer. Based on visual observations, the possible typical flow patterns in the downflow tube during the LBLOCA reflux stage are described. To study the influence of different injection methods and injection structures, a series of experiments were carried out on the descending section of a 1/8.5 ratio HPR1000 improved injection system under air and water flow conditions. The differences in the bypass characteristics of different safety injection modes were also discussed. According to the visualization results, the flow effect in the ring cavity of the descending section was analyzed, and the bypass mechanism was understood. On this basis, the Wallis parameter was derived as an important dimensionless parameter of the multidimensional ECC bypass phenomenon, and dimensionless parameter analysis was performed on the experimental results under different scale models.

2.Experimental facility and test conditions

The objective of the experiment is to study the re - injection stage of a large break accident in which a cold pipeline of the HPR1000 improved safety injection system completely ruptures, particularly the direct injection of emergency cooling water into the pressure vessel. The test was conducted on the air - water two - phase flow test platform of the Two - phase Flow and Interface Phenomena Laboratory at Chongqing University. The system circuit diagram is presented in Fig. 1, which includes electromagnetic flowmeters, thermal gas mass flowmeters, pressure differential pressure transmitters, and other measuring instruments.

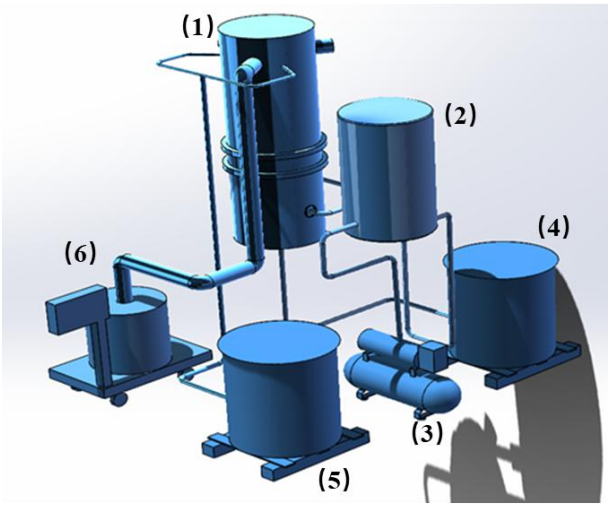

(a) Schematic diagram of experimental system：(1)downcomer,(2) air storage tank,(3) air compressor,(4) water storage tank,(5) recovery tank,(6) bypass flow tank

(b) Physical diagram of the experimental system

Fig.1 Experimental system

This test is based on the HPR1000 improved safety injection system as the prototype. The system adopts the pressure vessel direct injection (DVI) technology and is equipped with two rows of DVI nozzles. The pipe layout schematic diagram is shown in Fig. 2. Among them, DVI - 1 and DVI - 2 are two DVI pipes. CL1, CL2, and CL3 are three cold legs, each separated by 120°. The DVI nozzle is asymmetrical with the loop of the cold pipe section. Its elevation is 200 mm below the center line of the cold pipe section.

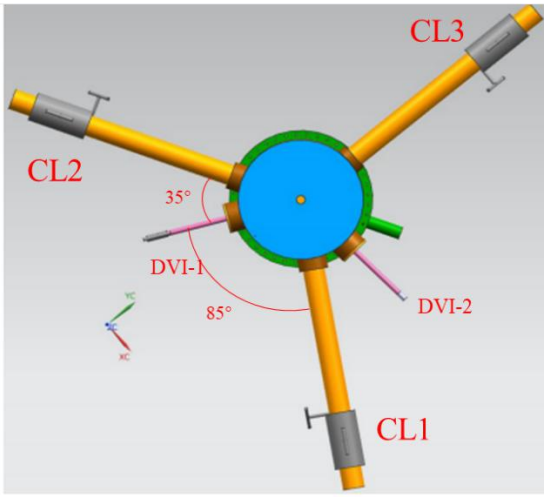

Fig.2 Nozzle distribution diagram

2.1. Scaling Methodology

Scale analysis is a method developed to construct a scaled test bench capable of simulating the prototype accident process. Its essence lies in simplifying the prototype system into a research model by reducing the scale and altering the fluid properties in accordance with the similarity theory, thereby achieving similarity between the model and the prototype. The model experimental research of nuclear reactor systems has a history of several decades and has mainly developed methods such as the linear proportional method, power - volume method, Ishii three - level method, H2TS proportional analysis method, and the improved linear method proposed by Korea for the CCFL phenomenon in the pressure vessel descent channel. Firstly, the main proportional relationships required for the application of various proportional methods in the system under isobaric and other physical property conditions are summarized. The main parameters of each modeling criterion method are presented in Table 1.

Table 1 Summary of main parameters of each modeling criterion method

Parameter	Linear method	Ishii	Improved linear method	H2TS
Length ratio,	l_R	l_R	l_R	l_R
Diameter ratio	l_R	d_R	l_R	$d_R=l_Rf_R$
Area ratio,	l_R^2	d_R^2	l_R^2	d_R^2
Volume ratio	l_R^3	$l_Rd_R^2$	l_R^3	$l_Rd_R^2$
Velocity ratio	1	$l_R^{1/2}$	$l_R^{1/2}$	$l_R^{1/2}$
Time ratio	l_R	$l_R^{1/2}$	$l_R^{1/2}$	$l_R^{1/2}$
Power/volume ratio	l_R^{-1}	$l_R^{-1/2}$	$l_R^{-1/2}$	$l_R^{-1/2}$
Flow rate ratio	l_R^2	$d_R^2l_R^{1/2}$	$l_R^{5/2}$	$d_R^2l_R^{1/2}$
Gravity ratio	l_R^{-1}	1	1	1

As can be observed from the above table, the differences among several

modeling methods are relatively small, mainly due to variations in the consideration of the diameter ratio. In this paper, the improved linear proportional modeling method is adopted for modeling. This method primarily commences from the momentum equation, performs dimensionless normalization on the momentum equation, and subsequently obtains a series of dimensionless criterion numbers. It is assumed that the fluid flow is two - dimensional and that the liquid phase flows down the wall upon entering the ring cavity. Additionally, the fluid flow is considered incompressible, and interfacial heat transfer is not taken into account.

Based on the test capacity, HPR1000 structural parameters, and corresponding operating flow, a fixed scale factor was determined for this test. Modeling calculations were carried out on the specific size and working conditions of the HPR1000' s RPV structure using the improved linear modeling criteria. In this study, the modeling ratio was selected to be 1/8.5. The specific parameters after modeling are presented in Table 2.

Table 2 The main scaling parameters

Structure	Prototype size	Modular size
Outside diameter of downcomer/mm	4246	500
Inside diameter of downcomer/mm	3750	441
Annular clearance /mm	248	29.5
Cold leg diameter /mm	760	89
DVI diameter /mm	150	18
Total length of RPV /mm	6596.2	776
Distance between cold leg and DVI tube center /mm	100	12
	200	23.5
	300	35
DVI tube center axial distance /mm	5069.6	596

2.2 Description of the Test Facility

The main part of the test section is depicted in Fig. 3. Since the test mainly simulates the process of water injection from the DVI nozzle to the RPV descending section during the water refill stage under large LOCA conditions, the test body primarily simulates the RPV descending section ring cavity, cold pipe section pipeline, DVI nozzle, and other structures. No simulation was conducted for the core and other components. The air compressor compresses the air and stores it in the gas reservoir. During the experiment, safe water is injected from the upper part of the test section, and air is injected from the lower part of the test section through the honeycomb rectifier to form a two - phase countercurrent with the safe water. To simulate large breaks in actual accident conditions, the ball valve connected to one of the three cold pipe sections will be fully opened during the experiment to achieve complete connection with the external environment, while the ball valves of the other two cold pipe sections will be fully closed to simulate a complete cold pipe section loop. Different break conditions are realized by fully opening or closing the ball valve,

ensuring that the break characteristics of each working condition remain consistent.

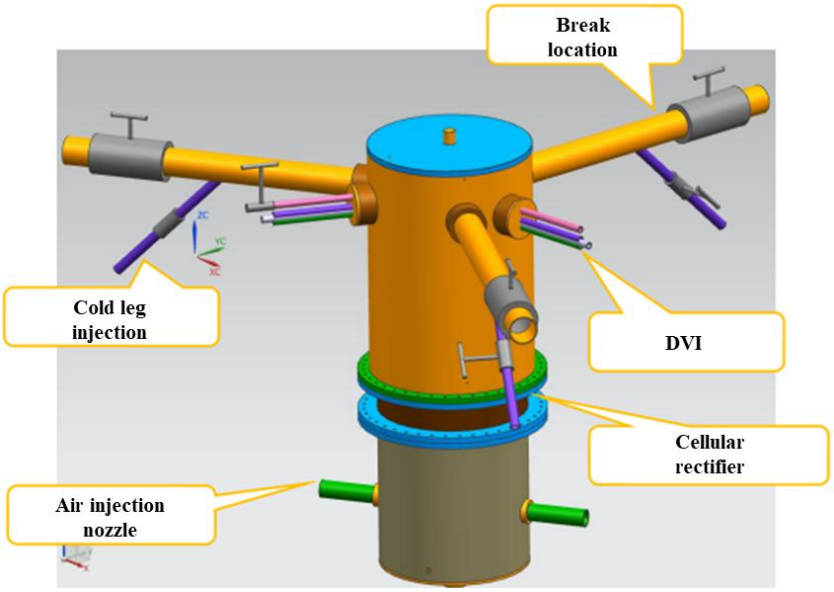

Fig.3 Test section diagram

2.3 Test Conditions

Based on the relevant structure and actual working conditions, three test conditions were designed: the comprehensive effect of DVI injection (Test A), the difference test between DVI injection and cold pipe section injection (Test B), and the influence of adding a diversion structure (Test C).

First, the actual test conditions of the reactor are presented in Table 3. Based on the actual working condition data and in accordance with the Wallis similarity criterion, the water injection and gas flow were modeled with a modeling ratio of $l_R^{5/2}$ (l_R is the geometric similarity ratio of 1/8.5). The liquid flow and air flow conditions of safety injection obtained in the relevant shrinkage test are shown in Table 4.

Table 3 Prototype test condition table

Times(s)	Safe injection liquid flow rate (kg/s)	Steam flow (kg/s)
14	120.846	820.838
15	612.072	790.678
17	874.222	727.997
19	1034.751	519.901
21	1139.988	319.468
25	1177.078	180.468
41	993.671	4.745

Table 4 Scale test condition table

Test condition							
Safety injection	0.569	1.389	2.083	2.883	4.153	4.527	5.556

flow/(kg/s)	
Air flow/(kg/s)	0-0.23

To investigate the influence of break locations on Direct Vessel Injection (DVI) performance, three cold leg (CL1, CL2, CL3) pipe rupture scenarios were simulated through valve actuation. Additionally, to compare flow characteristics between cold leg injection and DVI-based safety injection, a secondary experiment was conducted by deactivating the DVI system and rerouting injection through the intact cold legs. Furthermore, under the maximum bypass flow condition identified in the DVI tests, a geometrically scaled diversion structure (Fig. 4) was integrated into the annular cavity to evaluate its potential to mitigate injected water loss through the rupture site. These systematic tests aimed to optimize safety injection strategies under varying Loss-of-Coolant Accident (LOCA) scenarios.

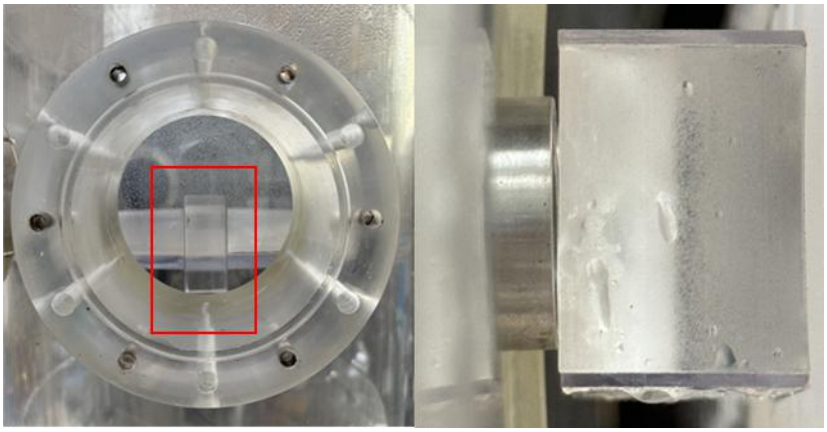

Fig.4 Schematic diagram of diversion structure

3.Experimental results and discussion

During the experiment, the liquid flow rate of safety injection, the liquid flow rate at the break, the gas flow rate injected from the lower nozzle of the steam injection pipe, and the pressure difference inside the ring cavity were measured. Three electromagnetic flowmeters of Honeywell with different ranges were used to measure the volume flow of water, with an accuracy of $\pm 0.5\%$. Their ranges were 100 - 1000 L/h, 600 - 12000 L/h, and 3 - 50 m^3/h, respectively, and the electrical signal range was 1.0 - 5.0V. The acquisition accuracy of the NI9220 data acquisition board is 1.37 mV, with a measuring range of 10.0 V, and the fluctuation of the mass flow rate is 0.02 V. Since the minimum measurable value of the electromagnetic flowmeter of the three ranges is 1.00V, the maximum uncertainty of the liquid phase flow measurement of the three meters is the same, which is calculated as follows:

$$\sigma_Q = \sqrt{\sigma_{instrument}^2 + \sigma_{\text{numerical sampling}}^2 + \sigma_{\text{fluctuation}}^2} = \sqrt{\left(\frac{5.00\times\frac{0.5}{100}}{1.00}\right)^2 + \left(\frac{1.37\times 0.001}{1.00}\right)^2 + \left(\frac{0.02}{1.00}\right)^2} = 3.20\% \quad (1)$$

Based on this calculation method, the gas phase flow uncertainty, pressure

uncertainty, and liquid phase flow uncertainty at the break were calculated, and the results were 1.57%, 2.03%, and 5.01%, respectively.

3.1 Bypass flow characteristic analysis

The characteristics of break bypass flow under different working conditions were analyzed to explore the differences in break bypass flow under the same safety injection flow but different safety injection methods.

Fig 5 presents the variation of the safety injection bypass flow with respect to the gas phase flow under diverse break conditions. Upon examination, it is evident that across different flow scenarios, the trend of change in the direct bypass flow as a function of the gas phase flow is largely consistent. When the gas phase flow rate reaches a specific value, the break bypass flow rate experiences a sudden increase. This abrupt rise indicates the occurrence of the counter current flow limitation (CCFL) phenomenon within the annular cavity. Moreover, as the gas phase flow continues to increase, the bypass flow also exhibits a gradual increase.

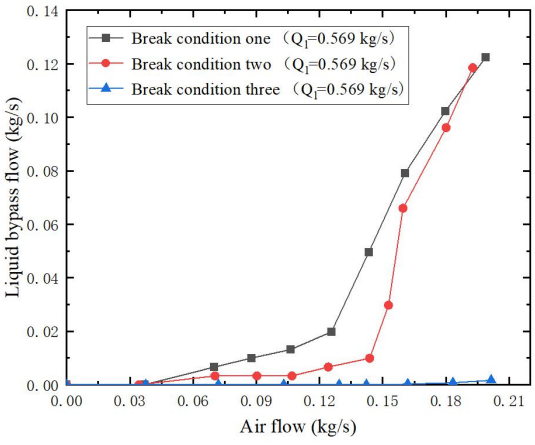

(a)Q_l=0.569 kg/s

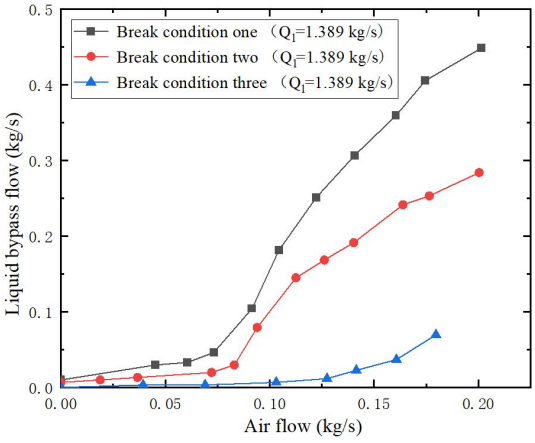

(b) Q_l=1.389 kg/s

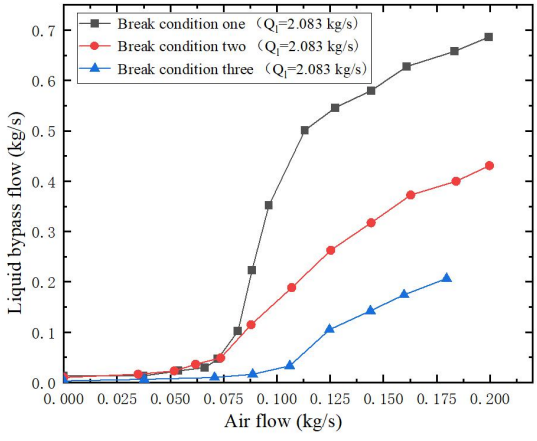

(c) Q_l=2.083 kg/s

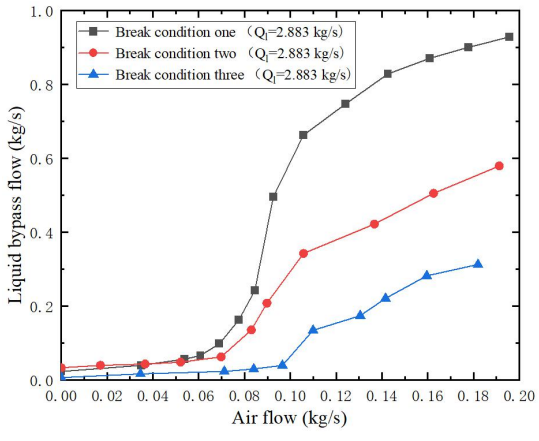

(d) Q_l=2.883 kg/s

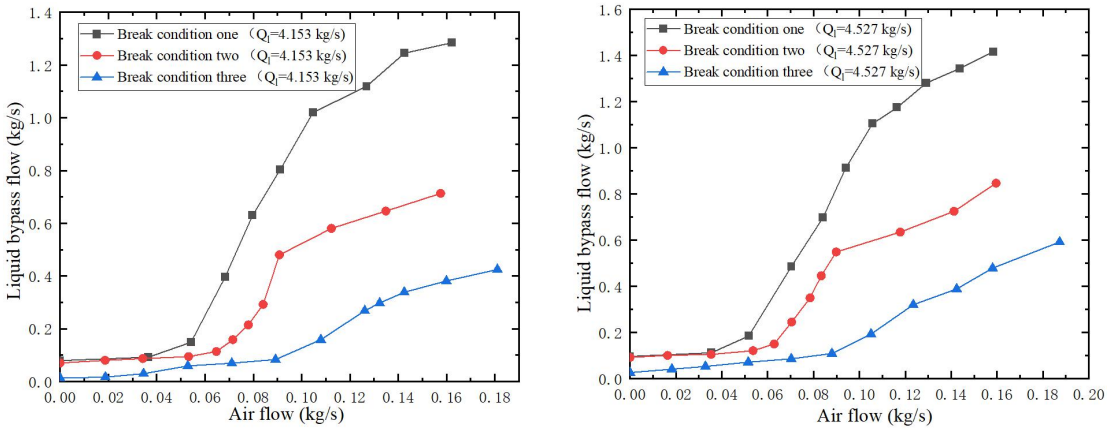

(e) Q_l=4.153 kg/s　　(f) Q_l=4.527 kg/s

Fig.5　Schematic diagram of diversion structure

Although the variation trends of bypass flow under different fracture conditions are generally similar, it has been observed that distinct fracture conditions are associated with different initiation points of the counter current flow limitation (CCFL). When CL1 experiences a break, it is positioned between two DVI nozzles. As a result, under this fracture condition, CCFL occurs at a relatively early stage, specifically when the liquid flow rate is at a minimum of 0.569 kg/s and the gas flow rate reaches 0.125 kg/s. In contrast, when compared to the CL3 fracture, no significant direct bypass flow is evident when the gas phase flow increases to 0.201 kg/s under the minimum flow condition. Moreover, under the same gas phase flow conditions, the bypass fractions of different breaks with direct bypass flow vary. For instance, at a gas flow rate of 0.160 kg/s, the bypass fraction corresponding to the maximum liquid phase flow rate of the CL1 fracture reaches 23%, whereas the bypass fraction corresponding to the largest liquid flow break in CL3 is merely 9%. This discrepancy can be attributed to the fact that under identical liquid flow conditions, the liquid film formed by the safe injection liquid phase upon impacting the inner wall of the annular cavity remains consistent. However, due to the varying positions of the breaks, the distances between the liquid film, its edge, and the break differ. Under conditions of high gas flow, a relatively low-pressure area forms around the break. In this low-pressure region, the gas phase entrains the safe injection liquid phase, thereby giving rise to the direct break side flow phenomenon.

Fig 6(a) illustrates the manner in which the proportion of the direct side flow of safe injection varies with the flow rate of safe injection and the gas phase flow under the cold leg safe injection condition. Upon analysis, it can be observed that across different flow scenarios, the trend of the direct bypass flow with respect to the gas phase flow bears a resemblance to that under the DVI safety injection condition. Notably, when compared to the DVI safety injection scenario, under the same liquid flow conditions, the gas flow requirements for the occurrence of the counter current flow limitation (CCFL) phenomenon in the cold pipe section differ significantly from those in the DVI safety injection condition. Under conditions of low liquid phase flow,

the cold pipe section safe injection exhibits no obvious fracture side flow phenomenon. Subsequent to the occurrence of CCFL and bypass flow, it has been determined that the proportion of bypass flow in the cold pipe section is relatively small. For example, when the gas phase flow ranges from 0.16 to 0.2 kg/s, the maximum bypass flow in DVI safety injection exceeds 1.4 kg/s, whereas in the cold pipe section, the maximum bypass flow amounts to only 0.3 kg/s.

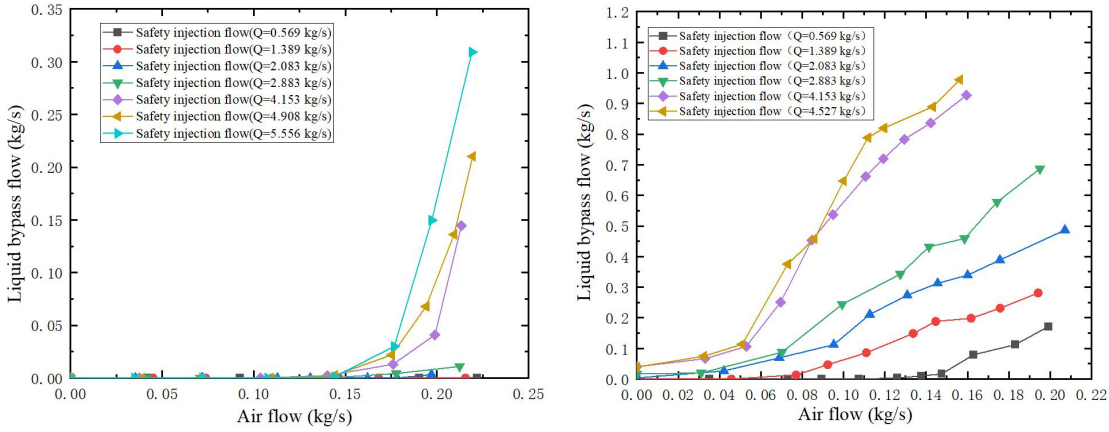

(a) Cold leg injection (b) Increasing diversion device

Fig.6 Change of bypass flow with cold leg injection and increasing diversion device

Fig 6(b) elucidates the variation of the proportion of the direct side flow of safety injection in relation to the safety injection flow rate and the gas phase flow rate when a diversion device is incorporated into the DVI safety injection system. When contrasted with the situation where no diversion device is present, it becomes evident that, under the same liquid flow conditions, the proportion of bypass flow at the break point where the counter current flow limitation (CCFL) occurs is remarkably decreased. The diversion device demonstrates a distinct guiding effect, capable of reducing the proportion of bypass flow by approximately 7% to 11%.

3.2 Visualization and flow effect analysis

To comprehensively investigate the behavior of water injection subsequent to its entry into the annular cavity, as well as the three-dimensional flow effects that manifest during the occurrence of the counter current flow limitation (CCFL) and fracture side flow phenomena, a high-speed camera was employed for image capture.

Fig 7 presents partial visual images of the DVI safety injection process. Specifically, images (a) and (b) depict the visual manifestations corresponding to the minimum safety injection flow under the CL2 fracture condition. As can be discerned from these images, when the gas phase flow rate is zero, the liquid phase emanates from the DVI nozzle and spreads to form a liquid film on the inner surface of the annular cavity. Once the gas flow rate increases to a specific level, the original state of the liquid film is entirely disrupted, and the liquid film in the vicinity of the fracture side is nearly completely fragmented. Consequently, the separated liquid phase is entrained by the gas phase and carried out of the test section from the location of the break.

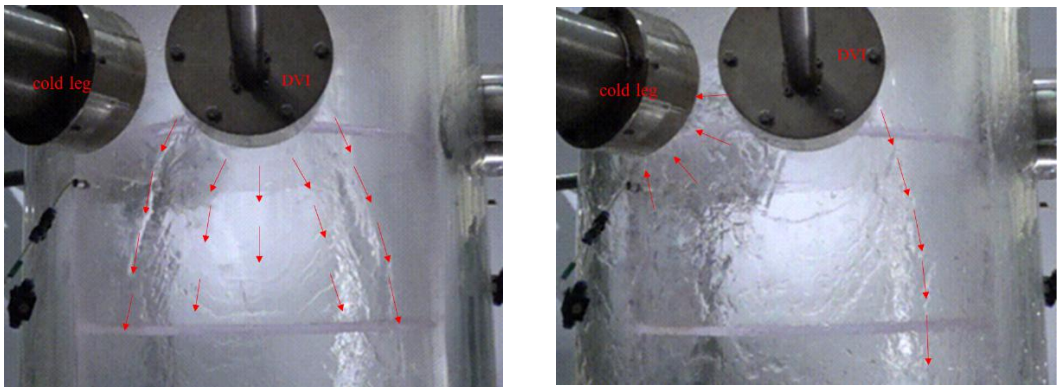

(a)Q_l=0.569 kg/s; Q_g=0 kg/s. (b) Q_l=0.569 kg/s; Q_g=0.198 kg/s.

Fig.7 Three-dimensional flow phenomenon in downcomer when DVI injection and CL1 fracture occurs

Fig 8 illustrates the three-dimensional flow phenomena within the annular cavity of the descending section during the cold leg injection process. As is evident from the visual imagery, following the injection of coolant, the edge of the liquid film does not approach the breach position in the same manner as in the case of DVI injection. This disparity can be attributed to the relatively large diameter of the three cold leg tubes and the 120° angular separation between them. Given that the edge of the liquid film is situated at a significant distance from the break position, upon an increase in the gas phase flow, the liquid phase that is broken and separated at the edge of the liquid film is not directly entrained by the gas phase. Instead, a majority of the liquid phase is entrained onto the wall below the break. Subsequently, due to the relatively low pressure effect existing at the break, this entrained liquid phase is sucked out of the test section.

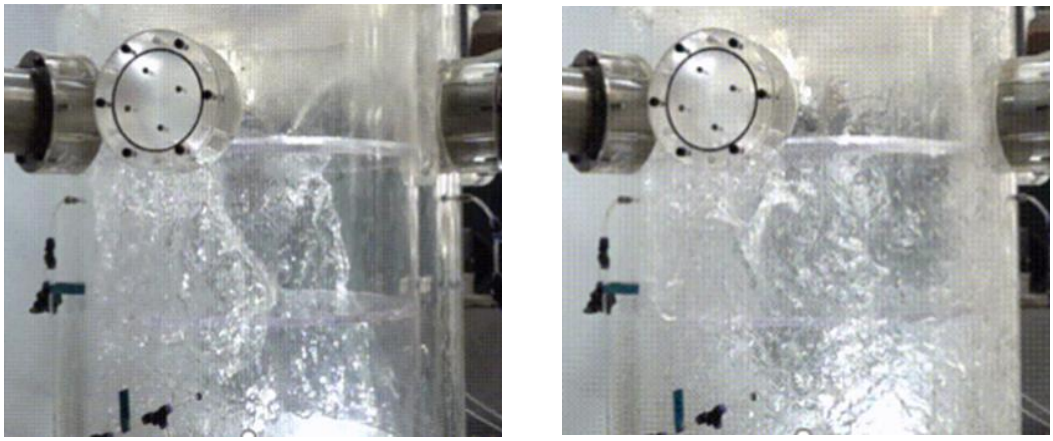

(a) Q_l=4.153 kg/s; Q_g=0 kg/s. (b) (b) Q_l=4.153 kg/s; Q_g=0.198 kg/s.

Fig.8 Three-dimensional flow phenomenon in downcomer during cold leg injection

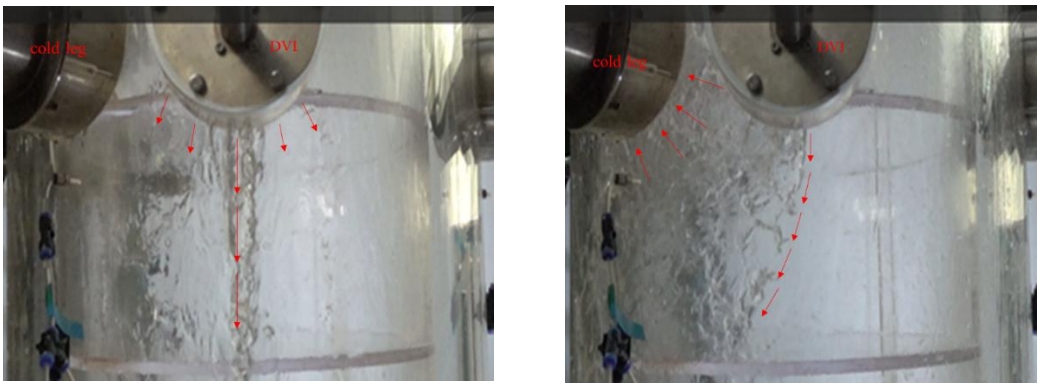

(a) (b) Q_l=0.569 kg/s; Q_g=0 kg/s. (b) (b) Q_l=0.569 kg/s; Q_g=0.198 kg/s.

Fig.9 Three-dimensional flow phenomenon in downcomer of the diversion device is added

As is apparent from Figure 9, upon the injection of the liquid phase into the annular cavity from the DVI tube nozzle, a portion of the liquid phase traverses down the flow channel of the diversion structure. Additionally, a small fraction of the liquid phase escapes from the flow channel and redistributes to form part of the liquid film prior to flowing downward. As the gas flow increases, the liquid column descending through the diversion device commences to deform and is induced by the gas phase to shift in the direction of the fracture. With a continuous increase in the gas flow rate, it is observed that the gas phase displaces the liquid column, and a portion of the liquid phase is propelled into the low-pressure region adjacent to the break, subsequently being carried out of the test section by the gas phase. When the gas phase flow rate is further increased to Q_g=0.199 kg /s, nearly all of the liquid phase is displaced and deviates towards the fracture direction. There is scarcely any liquid phase remaining on the right side below the water injection port. Moreover, the proportion of the liquid phase being carried out of the test section gradually rises with the increase in the gas phase flow rate.

3.3 Present countercurrent critical analysis

In an attempt to investigate the impacts of various factors on the initiation point of the counter current flow limitation (CCFL), the Wallis correlation form was utilized to conduct an analysis of the CCFL starting point. The principal approach involved transforming the apparent flow velocities of the gas - liquid phases into their corresponding dimensionless velocities. Subsequently, the apparent flow velocities of the CCFL starting points under different operating conditions were compared to elucidate the influence of the fracture location thereon. The dimensionless velocity is expressed as follows:

$$j_g^* = \frac{\rho_g^{0.5} j_g}{\left[gD\left(\rho_l - \rho_g\right)\right]^{0.5}} \quad (2)$$

$$j_l^* = \frac{\rho_l^{0.5} j_l}{\left[gD\left(\rho_l - \rho_g\right)\right]^{0.5}} \quad (3)$$

Where j_g^* and j_l^* represent the dimensionless apparent flow rates of the gas

phase and the liquid phase respectively. ρ_g and ρ_l are the density of gas phase and liquid phase respectively. j_g and j_l refer to the apparent flow rates of the gas phase and the liquid phase respectively. “D” is the feature length using the average perimeter of the annular channel; g stands for acceleration of gravity.

OMEGA mass flowmeter is used to measure the gas phase apparent flow rate, and its unit is SLM (standard liter per minute). To obtain the gas phase apparent flow rate under local conditions, the local pressure pi needs to be measured, which is:

$$j_g = \frac{\frac{M}{\rho_0} \cdot \frac{p_0}{p_i}}{A} \quad (4)$$

$$M = \frac{V - V_{\min}}{V_{\max} - V_{\min}} \times \left(M_{\max} - M_{\min} \right) \quad (5)$$

Where, M is the measured gas mass flow rate under the corresponding working condition, p_0 and p_i are the pressure under the standard condition and the pressure under the local working condition respectively, and are the gas phase density under the standard condition, A is the section area of the experiment section, $V_{\max}$ and $V_{\min}$ are the output voltage values corresponding to the maximum and minimum flow rate of the gas mass flowmeter respectively. $M_{\max}$ and $M_{\min}$ are the maximum and minimum ranges of the gas mass flowmeter respectively, and V is the output voltage value under the corresponding working conditions.

The apparent flow rate of the liquid phase is measured using an electromagnetic flowmeter. Given that the pressure undergoes minimal variation, the density of the liquid phase is assumed to be constant. Consequently, under fixed conditions, the apparent flow rate of the liquid phase remains invariant, as described below:

$$j_l = \frac{Q_l}{A} = \frac{V - V_{\min}}{V_{\max} - V_{\min}} \times \frac{\left(Q_{\max} - Q_{\min} \right)}{A} \quad (6)$$

Among them, $Q_{\max}$ and $Q_{\min}$ are the maximum and minimum measuring ranges of the flowmeter respectively, $V_{\max}$ and $V_{\min}$ are the output voltage values corresponding to the maximum and minimum measuring ranges of the flowmeter respectively, and Q_l is the liquid mass flow measured under the corresponding working conditions.

For the calculation of feature length D, there are:

$$D = 2\pi R_{\text{Average}} = 2\pi \left(\frac{D_{\text{Inside}} + D_{0\text{utside}}}{4} \right) \quad (7)$$

Where, D_{outside} and D_{inside} are the corresponding inner and outer diameters of the ring cavity channels respectively.

Fig 10 presents the outcomes subsequent to the dimensionless treatment of the CCFL starting points under diverse working conditions. An in-depth analysis of these results reveals that, under different fracture conditions, the dimensionless apparent velocity corresponding to the CCFL starting point exhibits a decreasing trend as the apparent velocity of the liquid phase increases. Moreover, when the liquid flow

conditions remain constant, the dimensionless apparent flow rates of the gas phase corresponding to CCFL vary across different fracture conditions.

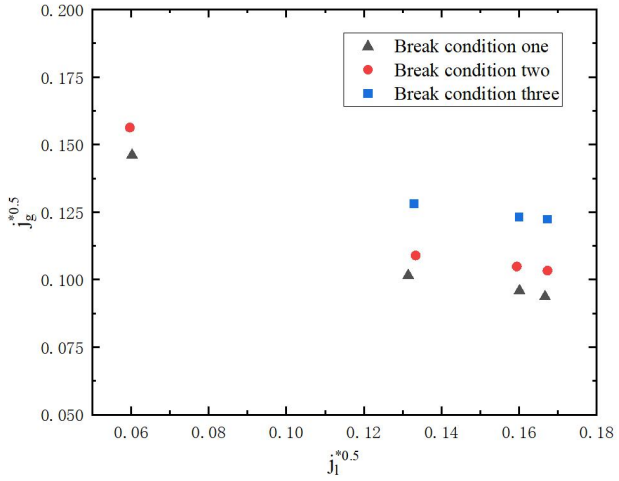

Fig.10 he starting point of CCFL changes with different fracture conditions

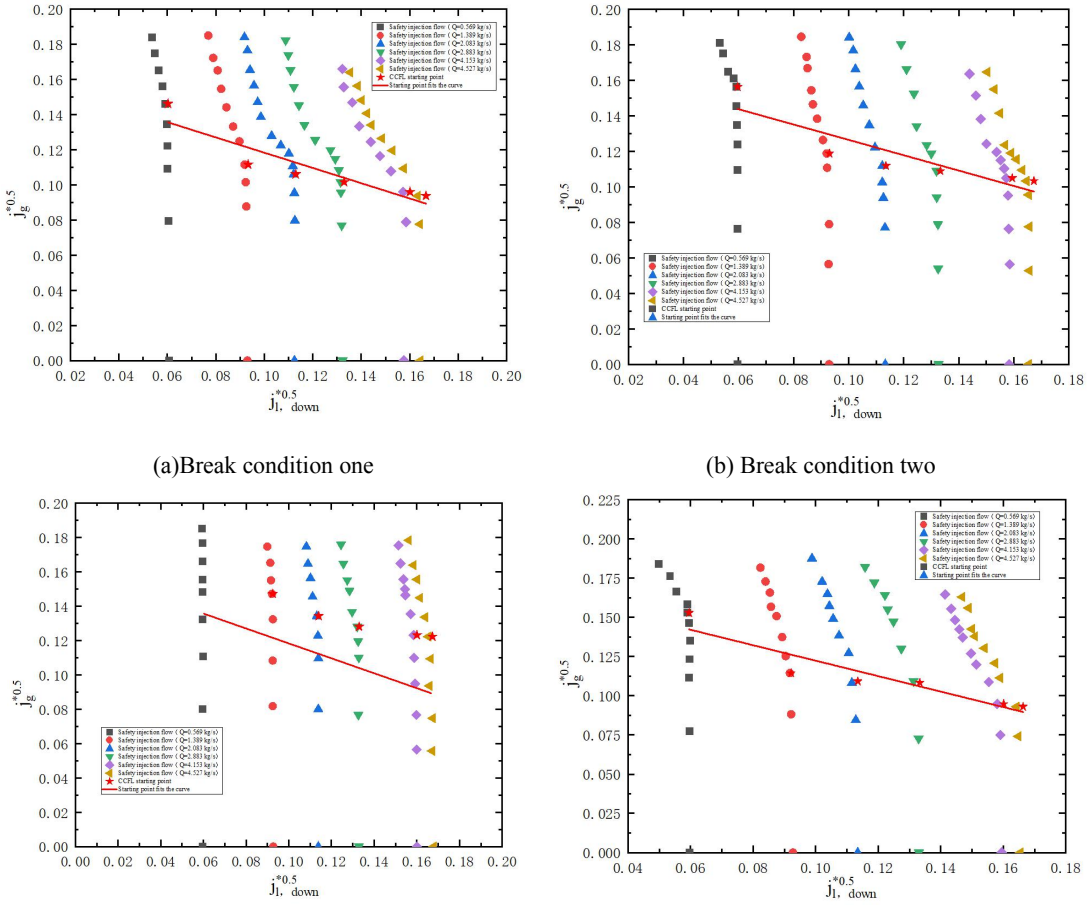

(a)Break condition one

(b) Break condition two

(c) Break condition three

(d) Break condition one- Increasing diversion device

Fig.10 Seepage flow and CCFL prediction curve

Fig 11 is constructed by employing the dimensionless apparent velocity of seepage flow. Additionally, the dimensionless apparent velocities of the gas - liquid two - phase are utilized to fit the Wallis relationship. The CCFL prediction

relationship derived from this fitting process can offer valuable references for predicting CCFL under pertinent accident conditions.

4. Conclusion

In this study, air was utilized as the medium, and the prototype device was modeled through the application of the improved linear method. Subsequently, the DVI safety injection side-flow tests were conducted under various working conditions during the recharging/reflooding stage of a large Loss of Coolant Accident (LOCA). The primary conclusions are outlined as follows:

(1) The spatial distance between the safety injection position and the break exerts a substantial influence on the alteration of the break's bypass flow rate. As the distance decreases, the phenomena of Counter Current Flow Limitation (CCFL) and bypass flow are more prone to occur. The primary source of bypass flow is the direct bypass flow. Notably, the proportion of bypass flow through the break is highly dependent on the distance from the break. For the same safety injection flow rate, the bypass flow shares near and far from the break are 23% and 9%, respectively.

(2) The CCFL and break side flow tests for loop injection in the cold pipe section were performed, and the obtained results were compared with those of DVI injection. The comparison indicates that, under identical liquid flow conditions, the gas flow required for the occurrence of CCFL and bypass flow in the cold pipe section is greater than that for DVI safety injection. Moreover, after the occurrence of CCFL, the proportion of bypass flow in the cold pipe section is relatively smaller.

(3) Experiments on CCFL and bypass flow, both with and without a diversion structure, were carried out, and the outcomes were compared with those of DVI injection. The comparison results demonstrate that, under low liquid flow conditions, the addition of the diversion device leads to an increase in the bypass flow under atmospheric phase flow conditions following CCFL. However, under high liquid phase flow conditions, the diversion device can effectively fulfill its diversion function, thereby reducing the share of direct bypass flow at the break. Specifically, the diversion effect can diminish the break's bypass flow by approximately 7% to 11%.

Acknowledgements

This work was supported by graduate research and innovation foundation of Chongqing, China [Grant Nos. CYB23036]

References

[1] Liao Q , Sun K .A new platform for clean energy and sustainable environment in the new era of decarbonization[J].DeCarbon, 2023, 1.

[2] MA Shengchao, YIN Huaqiang,HE Xuedong,et al. Safety Analysis of Break Loss of Coolant Accident of PWR Nuclear Power Plant [J].Atomic Energy Science and Technology,2019,53(06): 1036-1043.

[3] ZHANG Longfei, ZHANG Dafa ,et al. Study on serious accidents caused by large breach water loss accident of pressurized water reactor [J]. Atomic Energy Science and Technology,2007,(05):560-564.

[4] WU Lingjun,GUO Dingqing, et al. Study on measures of water injection in reactor cavity under severe accident of PWR nuclear power plant [J]. Atomic Energy Science and Technology, 2009, 43(1):5.

[5] Byong-Jo,Yun,Tae-Soon,et al.Air-Water Test on the Direct ECC Bypass During LBLOCA Reflood Phase with DVI[J].Nuclear Engineering and Technology, 2001.

[6] Lee D W , Hee Cheon N O , Kim H G ,et al.An Experimental Study of Thermal-hydraulic Phenomena in the Downcomer with a Direct Vessel Injection System of APR1400 during the LBLOCA Reflood Phase[J].Journal of Nuclear Science & Technology, 2004, 41(4):440-447.

[7] Cho H K , Yun B J , Song C H ,et al.Experimental validation of the modified linear scaling methodology for scaling ECC bypass phenomena in DVI downcomer[J].Nuclear Engineering & Design, 2005, 235(21):2310-2322.

[8] Kwon T S , Yun B J , Song C H ,et al.Effect of ECC Injection Angle on the Flow Distribution in a Downcomer Annulus During LBLOCA Reflood Phase in the Air-Water Test[J].american society of mechanical engineers, 2002.

[9] Yun B J , Euh D J , Song C H .Downcomer boiling phenomena during the reflood phase of a large-break LOCA for the APR1400[J].Nuclear Engineering & Design, 2008, 238(8):2064-2074.

[10] Cho S , Park H S , Choi K Y ,et al. CORE THERMAL HYDRAULIC BEHAVIOR DURING THE REFLOOD PHASE OF COLD-LEG LBLOCA EXPERIMENTS USING THE ATLAS TEST FACILITY[J].Nuclear Engineering & Technology, 2009, 41.DOI:10.5516/NET.2009.41.10.1263.

[11] Yoon, B. C,Ah, D. J,Joo, I. C, et al. UPTF Test 21D Counterpart Test in the MIDAS Test Facility under LBLOCA Late Reflood Phase[J]. 2003.

[12] Kwon T S , Song C H , Yun B J ,et al. Effect of the yaw injection angle on the ECC bypass in comparison with the horizontal DVI[J].Nuclear Engineering & Design, 2003,225(2/3):295-304.DOI:10.1016/S0029-5493(03)00182-1.

[13] Tae-Soon Kwon,Choeng-Ryul Choi,Chul-Hwa Song. Three-dimensional analysis of flow characteristics on the reactor vessel downcomer during the late reflood phase of a postulated LBLOCA[J].Nuclear Engineering & Design, 2003, 226(3): 255-265.

[14] Song C H , Park J K .Thermal-Hydraulic Experiments and the Evaluation of the New Safety Features in the APR1400[J].[2024-11-12].

[15] Kim W J , Suh K Y .Air–water multidimensional impingement flow on vertical flat wall[J].Nuclear Engineering & Design, 2009, 239(5):913-932.

[16] Yang J H , Euh D J , Cho H K ,et al. Development of wall and interfacial friction models for two-dimensional film flow with local measurement methods[J].Nuclear Engineering and Design, 2018, 336(SEP.):141-153.

[17] Park H S , Choi K Y , Cho S ,et al. Major findings from LBLOCA reflood tests using the ATLAS facility[J].Nuclear Engineering & Design, 2010, 240(12):3920-3929.

[18] Li Yuting. Charateristics of Countercurrent Critical Complex Interface Effects in Downcomer of Pressured Water Reactor [D]. North China Electric Power University,2022.

[19] CHEN Denggao, BI Jingliang, HUANG Yanping, et al. Study on CCFL Experiment and Model of Water-Steam in Downward Section of Reactor Pressure Vessel [J]. Atomic Energy Science and Technology, 2022, 56(6):11.

[20] Fei Likai, Zhang Peng, He Dandan, et al. Experimental Investigation of Counter-Current Flow in Downcomer of CAP1400 [J]. Nuclear Power Engineering, 2021, 42(2):5.

[21] Choi C J , Yang J H , Cho H K ,et al.Evaluation of Wall Friction Model in MARS-MultiD Module with Two-dimensional Film Flow Experiments[C]//International congress on advances in nuclear power plants, vol. 1: International congress on advances in nuclear power plants (ICAPP 2016), 17-20 April 2016, San Francisco, California, USA.2016.

[22] Ding Ke, Sun wan, Ding Shuhua, et al. Simulation Research on Counter Current Flow in Downcomer Annulus under Large Break Loss of Coolant Accident Condition [C]// The 16th National Reactor Thermal Fluid

Academic Conference and the 2019 Academic Annual Conference of CNNC Nuclear Reactor Thermal Hydraulic Technology Key Laboratory.0[2025-01-18].

[23] Li Xiang, Sun Wan, Ding Shuhua, et al. Study on CCFL Characteristics in Downcomer during Discharge Phase of LOCA with RELAP5 Code [J]. Nuclear Power Engineering, 2022(003):043.

[24] Miao Hongxing. AP1000 advanced nuclear power technology [J]. Automation Panorama1,2009,26(08):32-35.

[25] Lin Chengge. AP1000 Passive safety Advanced Nuclear Power Plant AP1000 [M]. Atomic energy Press,2008.

[26] Lee S S , Kim S H , Suh K Y .THE DESIGN FEATURES OF THE ADVANCED POWER REACTOR 1400[J].Nuclear Engineering & Technology, 2009, 41(8).DOI:10.5516/NET.2009.41.8.995.

[27] Zhou Linjun. Tianwan nuclear power plant VVER-1000 V428 unit introduction [R]. Beijing, 2018.

[28] LIANG Xiao，TAO Jun，WANG Qi，et al. An Scale Modeling and Visualized Experimental Study of Direct Vessel Injection of HPR1000 [J]. Nuclear Science and Engineering, 2022, 42(5):1133-1140.

[29] XIAO Weiming，PENG Fan，XING Jun, et al. Bypass and Heat Transfer Experiment Study of Direct Vessel Injection of HPR1000 [J]. Nuclear Science and Engineering, 2023, 43(6):1208-1215.